Tauroursodeoxycholic acid reduces apoptosis and protects against neurological injury after acute hemorrhagic stroke in rats

Cecilia M. P. Rodrigues*†, Susana Solá*†, Zhenhong Nan‡, Rui E. Castro†, Paulo S. Ribeiro†, Walter C. Low‡§, and Clifford J. Steer*¶‖

Departments of *Medicine, ¶Genetics, Cell Biology, and Development, and ‡Neurosurgery, and §Graduate Program in Neuroscience, University of Minnesota Medical School, Minneapolis, MN 55455; and †Centro de Patogénese Molecular, Faculdade de Farmácia, University of Lisbon, 1600-083 Lisbon, Portugal

Communicated by Eric M. Shooter, Stanford University School of Medicine, Stanford, CA, March 21, 2003 (received for review December 30, 2002)

Tauroursodeoxycholic acid (TUDCA), an endogenous bile acid, modulates cell death by interrupting classic pathways of apoptosis. Intracerebral hemorrhage (ICH) is a devastating acute neurological disorder, without effective treatment, in which a significant loss of neuronal cells is thought to occur by apoptosis. In this study, we evaluated whether TUDCA can reduce brain injury and improve neurological function after ICH in rats. Administration of TUDCA before or up to 6 h after stereotaxic collagenase injection into the striatum reduced lesion volumes at 2 days by as much as 50%. Apoptosis was ≈50% decreased in the area immediately surrounding the hematoma and was associated with a similar inhibition of caspase activity. These changes were also associated with improved neurobehavioral deficits as assessed by rotational asymmetry, limb placement, and stepping ability. Furthermore, TUDCA treatment modulated expression of certain Bcl-2 family members, as well as NF-κB activity. In addition to its protective action at the mitochondrial membrane, TUDCA also activated the Akt-1/protein kinase Bα survival pathway and induced Bad phosphorylation at Ser-136. In conclusion, reduction of brain injury underlies the wide-range neuroprotective effects of TUDCA after ICH. Thus, given its clinical safety, TUDCA may provide a potentially useful treatment in patients with hemorrhagic stroke and perhaps other acute brain injuries associated with cell death by apoptosis.

Apoptosis appears to play a key role in neuronal cell death from ischemic stroke (1–3). Bax, a proapoptotic member of the Bcl-2 family, is induced in the core (4) and in cells at the periphery of the infarct showing DNA fragmentation (5). In contrast, the antiapoptotic proteins Bcl-2 and Bcl-x_L are expressed in cells that are immediately adjacent to an infarct (6) and may survive ischemia (7). Caspase-3, the protease that plays a pivotal role in programmed cell death, is also activated in the ischemia-reperfusion injury (6). Together, these observations suggest that certain patterns of gene expression may reflect the fate of neurons in ischemic stroke. The mechanism of neuronal loss after hemorrhagic stroke is less well described, in part because of a lack of adequate experimental models. However, caspase inhibitors have recently been shown to inhibit DNA fragmentation after intracerebral hemorrhage (ICH) from collagenase injection into the rat striatum (8). Also, antisense inhibition of tumor necrosis factor-α reduced the number of apoptotic cells after ICH in rats (9).

It is well established that inflammation represents a key event in stroke, contributing to brain injury and perhaps modulating some of the identified pathways of cell death (10). NF-κB is a ubiquitous transcription factor that mediates a variety of proinflammatory responses (11). NF-κB in unstimulated cells is sequestered in the cytoplasm by the inhibitor protein IκB, which prevents its translocation to the nucleus. In response to various stimuli, including cytokines and reactive oxygen species, specific kinases phosphorylate IκB, leading to its proteolysis and dissociation from NF-κB. In the nucleus, NF-κB binds to specific response elements in the promoter of target genes, including proinflammatory cytokines but also antiapoptotic Bcl-2 elements. Activation of NF-κB can promote either cell injury or protection (12), and its specific function in stroke-induced injury remains unclear (13). Akt/protein kinase B is an upstream modulator of NF-κB and may play a key role in regulating neuronal cell death. In addition to phosphorylating IκB kinase-α (14), it also phosphorylates proapoptotic Bad, thereby blocking it from binding and inactivating antiapoptotic Bcl-2 and Bcl-x_L (15).

Ursodeoxycholic acid (UDCA) is an endogenous bile acid used during the past several decades for the treatment of certain liver diseases (16). More recently, it has been shown that UDCA and its conjugated derivative, tauroursodeoxycholic acid (TUDCA), play a unique role in modulating the apoptotic threshold in both hepatic and nonhepatic cells (17–19). They protect the mitochondrial membrane, thereby inhibiting mitochondrial membrane depolarization and channel formation, production of reactive oxygen species, release of cytochrome *c*, caspase activation, and cleavage of the nuclear enzyme poly-(ADP-ribose) polymerase (18, 20). They may also significantly modulate the mitogen-activated protein kinase survival pathway (21). Finally, TUDCA is neuroprotective not only in pharmacologic and transgenic animal models of Huntington disease (22, 23), but also for acute ischemic stroke (24). The bile acid reduced infarct size and improved neurological function, while significantly preserving mitochondrial membrane stability and inhibiting caspase activation.

This study was done to characterize further the role of apoptosis in ICH from collagenase injection and to identify the nature and mechanisms of TUDCA neuroprotection. We report that administration of the bile acid led to a marked reduction in neuronal cell death by apoptosis. Further, NF-κB activation was significantly decreased, Bcl-2 levels remained elevated, and rats showed improved neurological function. In addition, TUDCA resulted in Bad phosphorylation through activation of the Akt survival pathway. We conclude that TUDCA is a unique, nontoxic endogenous molecule that could potentially be a powerful therapeutic agent for the treatment of acute hemorrhagic stroke.

Materials and Methods

Rat Model of ICH. All animals received humane care in compliance with the institute's guidelines as outlined in "Guide for the Care and Use of Laboratory Animals" prepared by the National Academy of Sciences (NIH publication no. 86-23, revised 1985). Female Sprague–Dawley rats (250–300 g; Harlan Breeders, Indianapolis) were anesthetized with a mixture of ketamine and

Abbreviations: ICH, intracerebral hemorrhage; UDCA, ursodeoxycholic acid; TUDCA, tauroursodeoxycholic acid; TUNEL, terminal deoxynucleotidyltransferase-mediated dUTP end labeling; pNA, *p*-nitroanilide; bw, body weight.

‖To whom correspondence should be addressed. E-mail: steer001@tc.umn.edu.

xylazine and sat supine in a Kopf headholder. The right carotid artery was exposed and a PE-10 polyethylene tube (Becton-Dickinson) was introduced from the external into the internal carotid artery. Saline or TUDCA (Calbiochem–Novabiochem, San Diego), dissolved in phosphate buffer, pH 7.4 at 400 mg/ml, was slowly injected into the internal carotid at 1 ml/kg of body weight (bw). TUDCA at 10, 50, 100, or 200 mg/kg of bw was administered 1 h before, or 1, 3, and 6 h after collagenase injection.

Animals were placed in a stereotaxic apparatus to induce ICH by collagenase (25, 26). In brief, 2 μl (0.5 μl/min) of saline containing 0.5 units of bacterial collagenase (type VII; Sigma) was injected stereotaxically into the striatum at coordinates 0.4 mm anterior and 3.0 mm lateral to bregma and 5.0 mm ventral to the cortical surface. After injection, the Hamilton syringe was left in place for 3 min. Body temperature was maintained at 37°C with a CMA/150 temperature controller throughout the surgery. Neurological testing was performed at 2 days after ICH. The animals were then killed, and the brains removed and frozen at −70°C. In a subset of animals, serum and brain samples were collected for bile acid analysis.

Neurological Testing. The animals were tested for rotational behavior 2 days after ICH. Apomorphine (1 mg/kg of bw; Sigma) was injected s.c., and rotations were determined by a computer-controlled Columbus Instruments Videomex-V system (Columbus, OH). Counts were taken every 5 min and continued for 60 min. The limb placement protocol was modified from De Ryck (27) and consisted of six tests to evaluate forelimb and hindlimb function on each side of the body. Step initiation was assessed by stepping behavior of the left and right forelimbs. The animal is held in a manner that restrains one forelimb and both hindlimbs. The number of steps initiated by each limb was counted for 1 min.

Volume Determination. After behavioral testing, the brains were removed and fixed for cryostat sectioning. The lesions, including core and peri-ICH regions, were quantitated by using unbiased stereologic volumetric analysis (28) of Nissl-stained sections. The areas were determined in 11 sections from each animal 20 μm thick and 900 μm apart. Volumes (cubic millimeters) were calculated according to the formula $V = T \times a/p \times \Sigma Pi$, where V = volume of interest, T = distance between sections (millimeters), a/p = area associated with each point (square millimeters), and Pi = points hitting object in each section.

Terminal Deoxynucleotidyltransferase-Mediated dUTP End Labeling (TUNEL) Staining. Apoptotic cells were quantitated by using the TUNEL assay. Sections 10 μm thick were fixed with 1% formaldehyde and processed. An Apoptag *in situ* apoptosis detection kit (Intergen, Purchase, NY) was used for TUNEL staining. The number of TUNEL-positive cells was counted on a computer screen grid from at least three random fields (×400) within the region adjacent to the hemorrhagic core for each animal.

Asp-Glu-Val-Asp-Specific Caspase Activity. Tissues were homogenized in isolation buffer containing 10 mM Tris·HCl buffer, pH 7.6, 5 mM $MgCl_2$, 1.5 mM KAc, 2 mM DTT, and protease inhibitor mixture tablets (Complete; Roche Diagnostics). General caspase activity was evaluated by enzymatic cleavage of chromophore *p*-nitroanilide (pNA) from the substrate *N*-acetyl-Asp-Glu-Val-Asp-pNA (Sigma). The proteolytic reaction was conducted in isolation buffer containing 50 μg of cytosolic protein and 50 μM Asp-Glu-Val-Asp-pNA. The reaction mixtures were incubated at 37°C for 1 h, and the formation of pNA was measured at 405 nm with a 96-well plate reader. Protein concentrations were determined by using the Bio-Rad protein assay kit (Bio-Rad).

RNA Isolation and RT-PCR. Total RNA was extracted from tissue by using the TRIzol reagent from Life Technologies (Grand Island, NY). For RT-PCR, 5 μg of total RNA was reverse-transcribed with oligo(dT) (IDT, Coralville, IA) and SuperScript II reverse transcriptase (Life Technologies). Specific oligonucleotide primer pairs were incubated with cDNA template for PCR amplification by using the Expand High Fidelity PCR System from Roche Diagnostics. The following sequences were used as primers: Bcl-2 sense primer, 5′-CTGGTGGCAACATCGCTCTG-3′, and Bcl-2 antisense primer, 5′-GGTCTGCTGACCTCACTTGTG-3′; Bax sense primer, 5′-TGGTTGCCCTTTTCTACTTTG-3′, and Bax antisense primer, 5′-GAAGTAGGAAAGGAGGCCATC-3′; Bcl-x_L sense primer, 5′-AGGTCGGCGATGAGTTTGAA-3′, and Bcl-x_L antisense primer, 5′-CGGCTCTCGGCTGCTGCATT-3′; β-actin sense primer, 5′-TGCCCATCTATGAGGGTTACG-3′, and β-actin antisense primer, 5′-TAGAAGCATTTGCGGTGCACG-3′. The β-actin mRNA served as control. PCR products were analyzed by agarose gel electrophoresis and ethidium bromide staining.

Immunoblotting and Immunohistochemistry. Bcl-2 family, NF-κB, IκB, *p*-Akt, and *p*-Bad protein levels were determined from total protein homogenates separated by SDS/12% PAGE. Blots were probed with either primary mouse monoclonal antibodies reactive with Bcl-2 and NF-κB, or with rabbit polyclonal antibodies to Bcl-$x_{S/L}$, Bax, IκB, Ser-473 phosphorylated Akt-1 and Akt-2, and Ser-136 phosphorylated Bad at a dilution of 1:500 (Santa Cruz Biotechnology), and subsequently incubated with secondary anti-mouse or anti-rabbit antibodies conjugated with horseradish peroxidase. Finally, membranes were processed for proteins by using the SuperSignal substrate (Pierce). Immunohistochemistry of NF-κB activation was performed in coronal cryosections 10 μm thick by using the ImmunoCruz staining system (Santa Cruz Biotechnology). The sections were probed with an activation-specific monoclonal antibody to NF-κB p65 subunit (Santa Cruz Biotechnology), the epitope of which binds only after IκB dissociation, and detected with a secondary anti-mouse biotin-conjugated antibody. Multiple sections from each rat were examined in the region adjacent to the hematoma.

Bile Acid Analysis of Serum and Brain. Rats were killed 1, 3, and 6 h after TUDCA or vehicle injection. Blood was collected, clotted, spun, and the serum removed and frozen at −20°C. In addition, brains were removed after 5% chloral hydrate anesthesia and transcardial phosphate buffer perfusion, flash frozen, and stored at −70°C. Bile acids were assessed by gas chromatography after extraction, purification, hydrolysis, and derivitization (29).

Densitometry and Statistical Analysis. The relative intensities of the protein and nucleic acid bands were analyzed by using the IMAGEMASTER 1D ELITE densitometric analysis program (Amersham Pharmacia). Statistical analysis was performed by using GRAPHPAD INSTAT version 3.00 for WINDOWS 95 (GraphPad, San Diego) for the ANOVA and Bonferroni's multiple comparison tests.

Results

TUDCA Decreases Hematoma Volumes and Apoptosis. Nissl staining of serial sections revealed large hemorrhagic lesions in the right striatum 2 days after collagenase injection (Fig. 1). The volumes reflected the degree of striatal atrophy and the compensatory increases in ventricular size (data not shown). In addition, the hemorrhages were markedly reduced in animals that received TUDCA 1 h before collagenase. The lesions were ≈50% larger

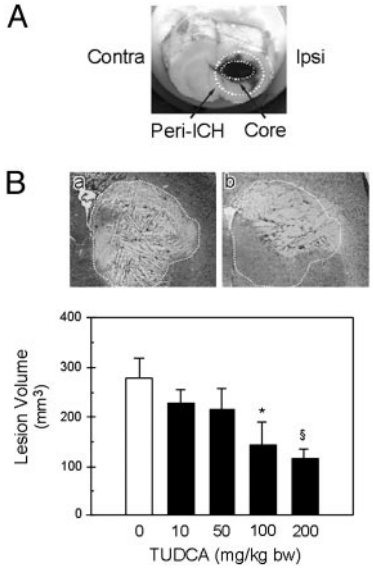

Fig. 1. Collagenase induces intrastriatal hemorrhage in rats. (*A*) Coronal section of the brain 2 days after ICH. The ipsilateral (Ipsi) ICH core and its periphery (Peri-ICH) are outlined. The contralateral (Contra) hemisphere was analyzed as control. (*B*) The total lesion volume was markedly reduced in animals receiving TUDCA (10–200 mg/kg of bw) given 1 h before collagenase. Representative Nissl-stained striatal sections are shown for each treatment group. The vehicle lesion (*a*) is outlined for reference and superimposed on the striatum of TUDCA animals (*b*). Quantitation of lesion volumes is the mean ± SEM ($n = 5$ animals per group). *, $P < 0.05$; §, $P < 0.01$ from vehicle.

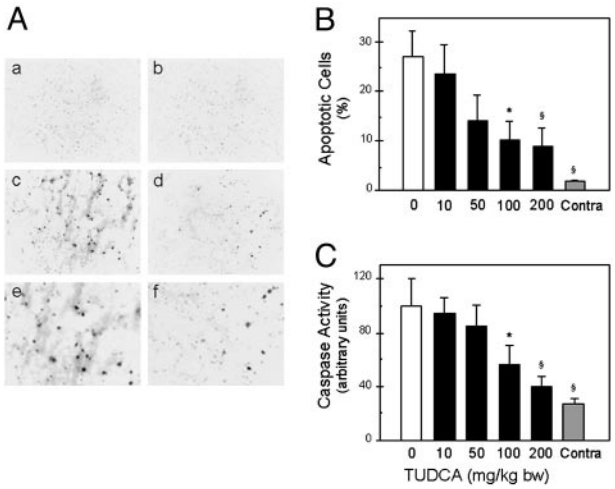

Fig. 2. TUDCA reduces apoptosis in the ICH hemisphere. (*A*) Rare TUNEL-positive cells were seen in the contralateral hemisphere with vehicle (*a*) and 100 mg/kg of bw TUDCA given 1 h before ICH (*b*). A marked increase was detectable in the ICH hemisphere of vehicle animals (*c*), and at higher magnification (*e*). TUDCA significantly reduced TUNEL reactivity (*d*), and at higher magnification (*f*). (Original magnification, ×200.) (*B*) Greater numbers of apoptotic cells were observed in vehicle rats than in TUDCA. Data are presented as the mean ± SEM ($n = 5$ animals per group). (*C*) Caspase activity was significantly increased in the vehicle controls and reduced with TUDCA. Data are the mean ± SEM ($n = 5$ animals per group). *, $P < 0.05$; §, $P < 0.01$ from vehicle.

in the vehicle-injected group than in the 100 mg/kg of bw TUDCA-treated rats (278.4 ± 39.2 mm^3 vs. 143.9 ± 46.5 mm^3; $P < 0.05$). At 200 mg/kg of bw TUDCA, a ≈60% reduction in lesion volume was also observed ($P < 0.01$), whereas 10 and 50 mg/kg of bw dose regimens were significantly less protective. Finally, there were fewer inflammatory cells in the peri-ICH region of the TUDCA animals (data not shown).

Few apoptotic cells were observed in the contralateral hemisphere in both groups (Fig. 2 *A* and *B*). However, TUNEL-positive cells were markedly increased in the ipsilateral hemisphere of vehicle-treated rats ($P < 0.01$). Electrophoresis of DNA from the ICH region also showed evidence of characteristic laddering into ≈200-bp fragments (data not shown). TUDCA reduced the number of apoptotic cells from almost 30% to ≈10% after 100 mg/kg of bw ($P < 0.05$). In addition, when administered at higher dosages, TUDCA reduced apoptosis by >65% ($P < 0.01$). Protein extracts were prepared and incubated with Asp-Glu-Val-Asp-pNA, a preferred substrate for caspase-3-like enzymes. Caspase activity in the contralateral hemispheres was similar to normal brain tissue (data not shown). In contrast, caspase activity was increased almost 4-fold in the ICH region of vehicle-injected rats ($P < 0.01$) (Fig. 2*C*). TUDCA reduced caspase activity by 45–60% with 100 ($P < 0.05$) and 200 mg/kg of bw ($P < 0.01$) dose. There were no differences between the hemispheres at the highest dose of TUDCA.

Next, we determined the therapeutic window for administration of TUDCA. Vehicle or TUDCA at 100 mg/kg of bw was injected 1 h before, or 1, 3, and 6 h after collagenase injection. At 2 days after ICH, lesions were markedly reduced in animals that received TUDCA 1 h before or up to 3 h after the hemorrhage ($P < 0.05$) (Fig. 3*A*). By 6 h, this 40–50% protective effect was partially reduced. Peri-ICH volumes, which represented up to 72% of the total hemorrhagic lesion, were decreased by TUDCA at all time points ($P < 0.05$) (Table 1). However, TUDCA provided no significant protection for the total lesion when given 6 h after the hemorrhage. TUNEL staining and caspase activity remained markedly lower in TUDCA animals throughout the time course (Fig. 3 *B* and *C*). Thus, in this model of acute hemorrhagic stroke, a window of at least 3 h existed for partial rescue from apoptosis.

TUDCA injection resulted in significantly increased bile acid concentrations in serum and brain. In fact, a single 100 mg/kg of bw dose resulted in an increase of bile acid in serum from 0.3

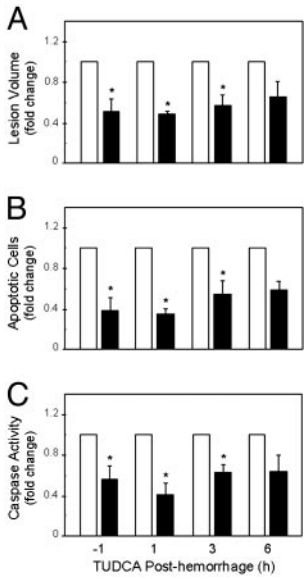

Fig. 3. TUDCA reduces lesion size and apoptosis after ICH. TUDCA at 100 mg/kg of bw (black bars), 1 h before or at up to 6 h after the ICH markedly reduced lesion volumes (*A*), TUNEL-positive cells (*B*), and caspase activation (*C*) in the ICH hemisphere, compared with vehicle controls (white bars). Data are the mean ± SEM ($n = 3$–5 animals per group). *, $P < 0.05$ from vehicle.

Table 1. Reduction of ICH core and its periphery (Peri-ICH) by TUDCA

Time TUDCA administration, h	Protection, %	
	ICH core	Peri-ICH
1	47.7 ± 3.2*	48.6 ± 3.5*
3	30.0 ± 18.9*	42.8 ± 14.9*
6	20.9 ± 12.9	38.7 ± 12.9*

Data are presented as mean ± SEM (n = 3–5 animals per group). *, $P < 0.05$ from vehicle at each time point.

to 10.6 μmol/liter even after 3 h. This change was associated with a 10-fold increase in brain concentrations compared with vehicle controls. In addition, an almost 2-fold elevation occurred in brain total bile acids in the stroke group compared with normal controls, which suggests an increased transport across the blood–brain barrier with ICH.

TUDCA Improves Neurological Function. TUDCA was also assessed for its effect on neurological function by using a variety of behavioral tests. In apomorphine-induced rotational asymmetry, the administration of TUDCA at 1, 3, or 6 h after ICH resulted in significant reductions in rotational bias (Fig. 4*A*). TUDCA administered after collagenase reduced rotational bias from 33.0 ± 12.1 to 2.3 ± 1.7 at 1 h; 54.6 ± 20.4 to 11.4 ± 5.6 at 3 h; 16.7 ± 1.8 to 4.3 ± 0.3 at 6 h ($P < 0.05$). In tests to assess neurological function by using the De Ryck scoring system (27), TUDCA increased neurological scores from 7.2 ± 0.6 to 10.8 ± 2.5 at 1 h after hemorrhage; 5.4 ± 0.7 to 10.4 ± 1.7 at 3 h ($P < 0.05$); and 7.0 ± 0.6 to 9.0 ± 1.0 ($P = 0.158$) at 6 h (Fig. 4*B*). Finally, in tests to assess forelimb stepping function, TUDCA reduced the difference between left and right forelimb steps from 3.1 ± 0.6 to 1.5 ± 0.6 ($P < 0.05$) at 1 h; 4.2 ± 0.4 to 3.4 ± 0.8 ($P = 0.199$) at 3 h; and 4.3 ± 0.9 to 2.3 ± 0.9 ($P = 0.184$) at 6 h.

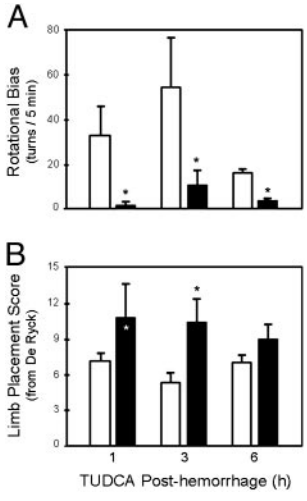

Fig. 4. TUDCA improves neurological function after ICH. (*A*) Rotational bias in rats with unilateral hemorrhage of the striatum was induced by apomorphine and evaluated in rats given TUDCA at 100 mg/kg of bw (black bars) or saline (white bars) at 1, 3, or 6 h after ICH. TUDCA animals in all groups displayed statistically significant reductions in rotational bias in comparison with their temporal control groups. (*B*) Limb placement in rats with unilateral hemorrhagic striatal injury was evaluated in rats given TUDCA (black bars) or saline (white bars) at 1, 3, or 6 h. TUDCA rats treated at 1 and 3 h exhibited significant improvements in limb placement scores. Data are presented as the mean ± SEM (n = 3–7 animals per group). *, $P < 0.05$ from respective controls.

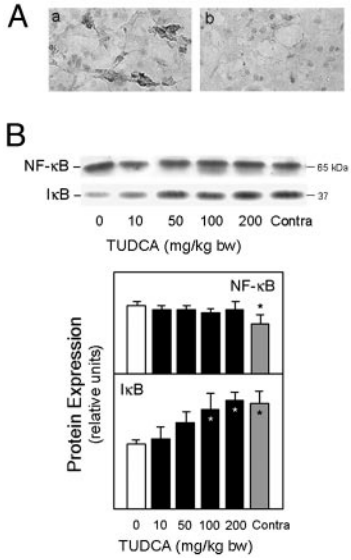

Fig. 5. TUDCA reduces NF-κB activation in ICH. (*A*) Striatal sections showing activation of NF-κB/p65 2 days after ICH. Immunoreactive NF-κB was clearly detectable in vehicle controls (*a*) but significantly reduced with 100 mg/kg of bw TUDCA given 1 h before ICH (*b*). (*B*) Representative immunoblot of p65 NF-κB subunit and IκBα and quantitation of changes in NF-κB/IκBα protein complex. Total protein extracts were subjected to SDS/PAGE, and the blots probed with antibodies to NF-κB/p65 and IκBα. TUDCA reduced the changes in NF-κB/IκBα protein expression from vehicle controls. Data are expressed as the mean ± SEM (n = 3–5 animals per group). *, $P < 0.05$ from vehicle.

NF-κB Activation Is Decreased by TUDCA. There were marked changes in NF-κB/IκBα protein complex in vehicles that were significantly reduced with TUDCA (Fig. 5). To assess NF-κB activation after ICH, we performed immunohistochemistry with an activation-dependent anti-NF-κB antibody. Immunoreactive NF-κB was clearly detectable in vehicles, whereas TUDCA markedly decreased NF-κB activation in the peri-ICH region (Fig. 5*A*). Further, the tissue distribution of NF-κB activation coincided with the TUNEL staining (data not shown). Western blot analysis for IκBα showed an almost 40% decrease in vehicle controls compared with the contralateral hemisphere ($P < 0.05$), and could be largely restored with TUDCA. Moreover, NF-κB p65 subunit expression was significantly increased ($P < 0.05$) in vehicles, which was unaffected by TUDCA (Fig. 5*B*).

The antiapoptotic Bcl-2 inhibits cytochrome *c* release from mitochondria (30, 31). Therefore, we examined whether ICH induces Bcl-2 protein as well as Bcl-x_L and Bax, relative to NF-κB activation (Fig. 6). Western blots revealed an increase of ≈6-fold in Bcl-2 protein levels ($P < 0.01$), and a less pronounced elevation in Bcl-x_L ($P < 0.05$) (Fig. 6*A*). Proapoptotic Bax was also significantly increased ($P < 0.05$). Bcl-2 protein levels with TUDCA did not correlate with NF-κB activation. Bcl-2 remained elevated throughout the study, whereas activation of the transcription factor was markedly reduced. Bcl-x_L protein levels were slightly diminished with TUDCA, whereas Bax protein returned to baseline values. RT-PCR analysis revealed a significant increase in *bcl*-2 ($P < 0.05$) and *bcl*-x_L ($P < 0.01$) mRNA levels, whereas *bax* mRNA was unchanged (Fig. 6*B*). TUDCA further increased transcriptional activation of Bcl-2, but decreased Bcl-x_L mRNA. These findings suggest that, in this model of ICH, up-regulation of Bcl-2 and Bcl-x_L expression is associated with NF-κB activation, which is reduced by TUDCA. Further, TUDCA is associated with increased production and/or stability of Bcl-2, probably through a pathway independent of NF-κB activation.

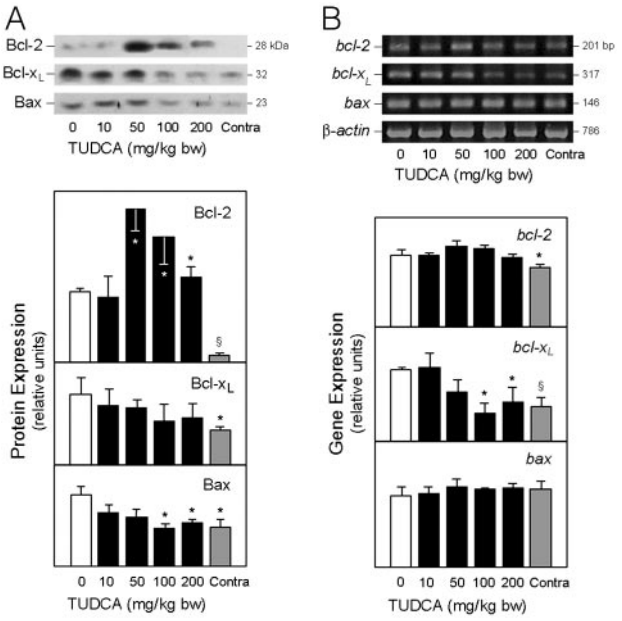

Fig. 6. TUDCA affects Bcl-2 family protein expression in ICH. (*A*) Total protein brain extracts underwent SDS/PAGE, and the blots were probed with antibodies to Bcl-2, Bcl-x_L, and Bax. All three proteins were elevated in vehicle controls. TUDCA (10–200 mg/kg of bw) given 1 h before ICH progressively decreased protein levels of Bcl-x_L and Bax, but not Bcl-2. (*B*) *Bcl-2*, *bcl-*x_L, and *bax* mRNAs were amplified by RT-PCR and analyzed by agarose gel electrophoresis and ethidium bromide staining. mRNA levels of *bcl-2*, *bcl-*x_L, and *bax* were increased in the vehicle-treated rats. Increasing doses of TUDCA progressively diminished *bcl-*x_L but not *bcl-2* transcriptional activity. The β-actin mRNA served as control. Data are presented as mean ± SEM (n = 3–5 animals per group). *, $P < 0.05$; §, $P < 0.01$ from vehicle.

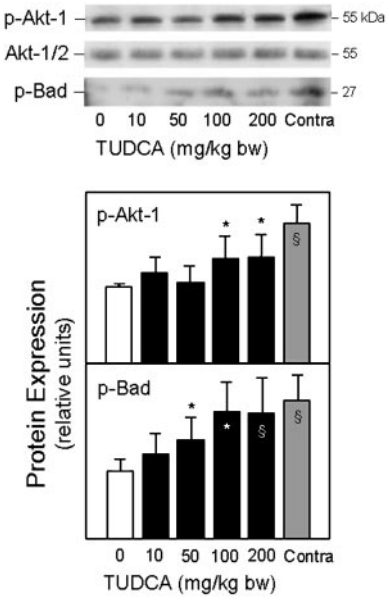

Fig. 7. TUDCA activates Akt in ICH. Total protein extracts were subjected to SDS/PAGE, and the blots were probed with antibodies to phosphorylated Akt and Bad. Both *p*-Akt-1 and *p*-Bad protein levels were decreased in the vehicle controls. TUDCA (10–200 mg/kg of bw) was given in increasing doses 1 h before ICH. Representative immunoblots and quantitation of respective protein levels show increasing Akt and Bad phosphorylation with dose. Data are presented as mean ± SEM (n = 3–5 animals per group). *, $P < 0.05$; §, $P < 0.01$ from vehicle.

TUDCA Increases Levels of Phosphorylated Akt and Bad in ICH. Akt, the cellular homolog of the viral oncoprotein v-Akt suppresses apoptosis. Akt has also been implicated in the phosphorylation of Bad (*p*-Bad), potentially linking survival pathways with the Bcl-2 family. We found that the expression of the phosphorylated form of Akt-1 was markedly decreased in ICH ($P < 0.01$), but could be largely restored by TUDCA (Fig. 7). Similarly, levels of *p*-Bad were almost 2-fold elevated with TUDCA, compared with vehicle controls ($P < 0.05$). We also tested whether the phosphatidylinositide 3′-OH kinase pathway is modulated by TUDCA. Isolated neurons were incubated with wortmannin, a selective inhibitor of phosphatidylinositide 3′-OH kinase, to block the phosphorylation of Akt by TUDCA. In fact, the inhibition of Akt phosphorylation resulted in significantly decreased cell viability (data not shown).

Discussion

ICH remains a devastating cerebrovascular event with a mortality rate approaching 50% (32, 33). Therapies have been largely ineffective in reducing morbidity and mortality, and clinical trials have lagged far behind those for patients with ischemic stroke. Injury is thought to arise from tissue reaction secondary to the hematoma resulting in ischemia, edema, intense inflammation (34), and ultimately cell death. Cell death from acute stroke is a complex process involving several different pathways. In the ischemia/reperfusion injury, neurons exhibit several features of apoptosis including chromatin condensation, TUNEL labeling, and activation of caspases (35). Characteristic changes of apoptosis have also been described after hemorrhagic stroke (36, 37). We also detected dramatically increased numbers of TUNEL-positive cells, and significant caspase activation in the region immediately surrounding the hematoma. This narrow zone of selective neuronal injury may significantly add to the area of stroke injury unless rescued from apoptosis. In fact, animals treated with caspase inhibitors and genetically engineered caspase-deficient mice showed reduced cell death from ischemic stroke (38–41).

In contrast to hydrophobic bile acids such as deoxycholic acid, UDCA and TUDCA are nontoxic and can act as antiapoptotic agents (17, 20). They directly inhibit reactive oxygen species production, collapse of the transmembrane potential, and disruption of the outer mitochondrial membrane (42). Both bile acids mitigate mitochondrial insufficiency and toxicity by inhibiting Bax translocation from cytosol to mitochondria (18, 20). Membrane stability inhibits cytochrome *c* release, thereby reducing downstream events such as caspase activation and substrate cleavage (43). In addition, TUDCA can inhibit endoplasmic reticulum stress-induced cell death by blocking a calcium-mediated apoptotic pathway (44).

We have recently shown that administration of TUDCA to a transgenic mouse model of Huntington disease significantly reduced striatal degeneration and improved locomotor and sensorimotor deficits (23). Furthermore, TUDCA reduced apoptosis, infarct volumes, and neurobehavioral impairment in an ischemia/reperfusion model of stroke (24). The present study extends our previous reports and shows a neuroprotective effect of TUDCA in an ICH model of stroke. TUDCA at superphysiologic doses significantly reduced the appearance of TUNEL-positive cells, activation of caspase-3-like proteases, and histological damage of the peri-ICH region. In addition, the tissue and biochemical changes were also associated with improved neurological function. Further, our data suggest that many neurons can be rescued with TUDCA by 3 h, and some up to 6 h after ICH. In fact, TUDCA administered up to 3 h after ICH significantly reduced the striatal lesions. Thus, many cells are able to be rescued for hours before cell death.

It is now well established that NF-κB activation may play a prominent role in acute stroke injury (13). NF-κB activation increases transcription of several different genes, including those involved in inflammation as well as apoptosis. The precise role of NF-κB in stroke, however, remains unclear. In fact, some studies suggest that NF-κB activation mediates injury, probably in response to both necrosis and apoptosis, whereas others suggest a protective role. NF-κB DNA-binding activity is increased after experimental ICH and activation is frequently colocalized to cells containing fragmented DNA (45), suggesting a proapoptotic role. Also, reducing expression of the proinflammatory cytokine tumor necrosis factor-α, a key mediator of NF-κB activation, has been shown to be neuroprotective after ICH (9). We detected significant activation of NF-κB in the region immediately surrounding the hematoma at 2 days after ICH. In addition, we also determined that downstream target genes of NF-κB encoding for the antiapoptotic protein Bcl-2, and to a lesser extent Bcl-x_L, were highly expressed in the same region.

These results suggest the activation of certain survival pathways to protect the brain against the proinflammatory response that contributes to cell injury in ICH. Bcl-2 levels remained elevated after TUDCA treatment despite a significant decrease in NF-κB activity. Thus, in the setting of ICH, the initial proinflammatory response and/or oxidative stress induces NF-κB activation that increases Bcl-2 and Bcl-x_L expression, thereby inhibiting apoptosis. Simultaneously, injury is exacerbated through the activation of other genes that mediate cell death. Indeed, we clearly show that apoptosis is still a prominent form of cell death in the peri-ICH region. By preventing the initial injury through stabilization of the mitochondrial membrane, TUDCA might indirectly decrease NF-κB activation. Simultaneously, we demonstrated that Bcl-2 levels remain elevated probably through the activation of alternative survival pathways by TUDCA. This study confirms that the signaling cascades that have been characterized in a variety of different cell types (46) are functional in the rat brain and can be modulated by TUDCA. More importantly, these pathways appear to be required for its neuroprotective effect. The single modification of Akt-mediated Bad phosphorylation can promote survival by disrupting Bad's ability to bind and inactivate Bcl-2 antiapoptotic proteins (47). Although it is not entirely clear how TUDCA reduces NF-κB activation, the modulation of protein kinase pathways alters cell survival in hemorrhagic stroke.

In conclusion, our results suggest that TUDCA can significantly reduce the injury associated with ICH. It appears to inhibit apoptosis by preserving mitochondrial membrane stability, as well as through activation of certain survival pathways. The marked antiapoptotic properties of TUDCA together with its lack of toxicity and potential use up to 6 h after injury make it an attractive candidate in the treatment of hemorrhagic stroke, as well as perhaps other acute neurological disorders, such as head and spinal cord injuries.

We thank Betsy T. Kren for critical review of the manuscript and Dora Brites for use of the gas chromatographer. This work was supported in part by the Lyle French Fund (to W.C.L.) and by Grant POCTI/BCI/44929/02 and Postdoctoral Fellowship PRAXIS XXI/BPD/11849/97 from Fundação para a Ciência e a Tecnologia, Lisbon (to C.M.P.R.). S.S. and R.E.C. were recipients of Ph.D. fellowships (SFRH/BD/4823/01 and SFRH/BD/10806/02) from Fundação para a Ciência e a Tecnologia.

1. Linnik, M. D., Zobrist, R. H. & Hatfield, M. D. (1993) *Stroke* **24,** 2002–2009.
2. MacManus, J. P., Buchan, A. M., Hill, I. E., Rasquinha, I. & Preston, E. (1993) *Neurosci. Lett.* **164,** 89–92.
3. Li, Y., Chopp, M., Jiang, N., Yao, F. & Zaloga, C. (1995) *J. Cereb. Blood Flow Metab.* **15,** 389–397.
4. Gillardon, F., Lenz, C., Waschke, K. F., Krajewski, S., Reed, J. C., Zimmermann, M. & Kuschinsky, W. (1996) *Mol. Brain Res.* **40,** 254–260.
5. Isenmann, S., Stoll, G., Schroeter, M., Krajewski, S., Reed, J. C. & Bähr, M. (1998) *Brain Pathol.* **8,** 49–63.
6. Asahi, M., Hoshimaru, M., Uemura., Y., Tokime, T., Kojima, M., Ohtsuka, T., Matsuura, N., Aoki, T, Shibahara, K. & Kikuchi, H. (1997) *J. Cereb. Blood Flow Metab.* **17,** 11–18.
7. Chen, J., Graham, S. H., Nakayama, M., Zhu, R. L., Jin, K., Stetler, R. A. & Simon, R. P. (1997) *J. Cereb. Blood Flow Metab.* **17,** 2–10.
8. Matsushita, K., Meng, W., Wang, X., Asahi, M., Asahi, K., Moskowitz, M. A. & Lo, E. H. (2000) *J. Cereb. Blood Flow Metab.* **20,** 396–404.
9. Mayne, M., Ni, W., Yan, H. J., Xue, M., Johnston, J. B., Del Bigio, M. R., Peeling, J. & Power C. (2001) *Stroke* **32,** 240–248.
10. Arvin, B., Neville, L. F., Barone, F. C. & Feuerstein, G. Z. (1996) *Neurosci. Biobehav. Rev.* **20,** 445–452.
11. Ghosh, S.& Karin, M. (2002) *Cell* **109,** S81–S96.
12. Li, N. & Karin M. (1999) *FASEB J.* **13,** 1137–1143.
13. Sharp, F. R., Lu, A., Tang, Y. & Millhorn, D. E. (2000) *J. Cereb. Blood Flow Metab.* **20,** 1011–1032.
14. Ozes, O. N., Mayo, L. D., Gustin, J. A., Pfeffer, S. R., Pfeffer, L. M. & Donner, D. B. (1999) *Nature* **401,** 82–85.
15. Datta, S. R., Dudek., H., Tao., X., Masters, S., Fu, H., Gotoh, Y. & Greenberg, M. E. (1997) *Cell* **91,** 231–241.
16. Paumgartner, G. & Beuers, U. (2002) *Hepatology* **36,** 525–531.
17. Rodrigues, C. M. P., Fan, G., Ma, X., Kren, B. T. & Steer, C. J. (1998) *J. Clin. Invest.* **101,** 2790–2799.
18. Rodrigues, C. M. P., Linehan-Stieers, C., Keene, C. D., Ma, X., Kren, B. T., Low, W. C. & Steer, C. J. (2000) *J. Neurochem.* **75,** 2368–2379.
19. Rodrigues, C. M. P., Solá, S. & Brites, D. (2002) *Hepatology* **35,** 1186–1195.
20. Rodrigues, C. M. P., Ma, X., Linehan-Stieers, C., Fan, G., Kren, B. T. & Steer, C. J. (1999) *Cell Death Differ.* **6,** 842–854.
21. Qiao, L., Yacoub, A., Studer, E., Gupta, S., Pei, X. Y., Grant, S., Hylemon, P. B. & Dent, P. (2002) *Hepatology* **35,** 779–789.
22. Keene, C. D., Rodrigues, C. M. P., Eich, T., Linehan-Stieers, C., Abt, A., Kren, B. T., Steer, C. J. & Low, W. C. (2001) *Exp. Neurol.* **171,** 351–360.
23. Keene, C. D., Rodrigues, C. M. P., Eich, T., Chhabra, M. S., Steer, C. J. & Low, W. C. (2002) *Proc. Natl. Acad. Sci. USA* **99,** 10671–10676.
24. Rodrigues, C. M. P., Spellman, S. R., Solá, S., Grande, A. W., Linehan-Stieers, C., Low, W. C. & Steer, C. J. (2002) *J. Cereb. Blood Flow Metab.* **22,** 463–471.
25. Rosenberg, G. A., Mun-Bryce, S., Wesley, M. & Kornfeld, M. (1990) *Stroke* **21,** 801–807.
26. Chesney, J. A., Kondoh, T., Conrad, J. A. & Low, W. C. (1995) *Stroke* **26,** 312–316.
27. De Ryck, M. (1990) *Eur. Neurol.* **30,** Suppl. 2, 21–27.
28. Howard, C. V., Howard, V. & Reed, M. G. (1998) *Unbiased Stereology: Three-Dimensional Measurement in Microscopy* (BIOS Scientific, New York).
29. Setchell, K. D. R., Rodrigues, C. M. P., Clerici, C., Morelli, A., Gartung, C. & Boyer, J. L. (1997) *Gastroenterology* **112,** 226–235.
30. Kluck, R. M., Bossy-Wetzel, E., Green, D. R. & Newmeyer, D. D. (1997) *Science* **275,** 1132–1136.
31. Yang, J., Liu, X., Bhalla, K., Kim, C. N., Ibrado, A. M., Cai, J., Peng, T. I., Jones, D. P. & Wang, X. (1997) *Science* **275,** 1129–1132.
32. Hankey, G. J. & Hon, C. (1997) *Stroke* **28,** 2126–2132.
33. Juvela, S. (1995) *Arch. Neurol.* **52,** 1193–1200.
34. Mendelow, A. D. (1993) *Stroke* **24,** 115–117.
35. Choi, D. W. (1996) *Curr. Opin. Neurobiol.* **6,** 667–672.
36. Gong, C., Boulis, N., Qian, J., Turner, D. E., Hoff, J. T. & Keep, R. F. (2001) *Neurosurgery* **48,** 875–882.
37. Matz, P. G., Lewen, A. & Chan, P. H. (2001) *J. Cereb. Blood Flow Metab.* **21,** 921–928.
38. Loddick, S. A., MacKenzie, A. & Rothwell, N. J. (1996) *NeuroReport* **7,** 1465–1468.
39. Cheng, Y., Deshmukh, M., D'Costa, A., Demaro, J. A., Gidday, J. M., Shah, A., Sun, Y., Jacquin, M. F., Johnson, E. M., Jr., & Holtzman, D. M. (1998) *J. Clin. Invest.* **101,** 1992–1999.
40. Endres, M., Namura, S., Shimizu-Sasamata, M., Waeber, C., Zhang, L., Gómez-Isla, T., Hyman, B. T. & Moskowitz, M. A. (1998) *J. Cereb. Blood Flow Metab.* **18,** 238–247.
41. Rabuffetti, M., Sciorati, C., Tarozzo, G., Clementi, E., Manfredi, A. A. & Beltramo, M. (2000) *J. Neurosci.* **20,** 4398–4404.
42. Rodrigues, C. M. P., Solá, S., Brito, M. A., Brondino, C. D., Brites, D. & Moura, J. J. G. (2001) *Biochem. Biophys. Res. Commun.* **281,** 468–474.
43. Benz, C., Angermüller, S., Töx, U., Klöters-Plachky, P., Riedel, H. D., Sauer, P., Stremmel, W. & Stiehl, A. (1998) *J. Hepatol.* **28,** 99–106.
44. Xie, Q., Khaoustov, V. I., Chung, C. C., Sohn, J., Krishnan, B., Lewis, D. E. & Yoffe, B. (2002) *Hepatology* **36,** 592–601.
45. Hickenbottom, S. L., Grotta, J. C., Strong, R., Denner, L. A. & Aronowski, J. (1999) *Stroke* **30,** 2472–2477.
46. Ihle, J. N. (1995) *Nature* **377,** 591–594.
47. Datta, S. R., Brunet, A. & Greenberg, M. E. (1999) *Genes Dev.* **13,** 2905–2927.